JOURNAL OF NATURAL PRODUCTS

pubs.acs.org/jnp

Article

Spirovetivane- and Eudesmane-Type Sesquiterpenoids Isolated from the Culture Media of Two Cyanobacterial Strains

Timothy J. O'Donnell, Yuheng Luo, Wesley Y. Yoshida, Sayuri Suzuki, Rui Sun, and Philip G. Williams*

Cite This: *J. Nat. Prod.* 2022, 85, 415−425

Read Online

ACCESS | Metrics & More | Article Recommendations | Supporting Information

ABSTRACT: As part of a study examining polar metabolites produced by cyanobacterial strains, we examined media extracts of a *Calothrix* sp. (strain R-3-1) and a *Scytonema* sp. (strain U-3-3). The cell mass of each was separated from the media, and HP20 resin was added for adsorption of secreted metabolites, a relatively unexplored area of cyanobacterial chemistry. HPLC-UV-LCMS-guided isolation led to the discovery of seven sesquiterpenoid compounds with five new, one known, and one previously isolated as the methyl ester. Through a complement of 1D and 2D NMR spectroscopic techniques, the planar structures and relative configurations of the seven compounds were elucidated. Spironostoic acid (**1**), 11,12-didehydrospironostoic acid (**2**), and 12-hydroxy-2-oxo-11-*epi*-hinesol (**4**) are spirovetivane-type compounds from R-3-1, while stigolone (**5**), 11*R*,12-dihydroxystigolone (**6**), and 11*S*,12-dihydroxystigolone (**7**) are three eudesmane-type compounds from U-3-3. Circular dichroism was utilized to decipher the absolute configurations of new compounds **1**, **2**, **4**, **5**, **6**, and **7**. Due to the structural variety observed among the spirovetivane- and eudesmane-type compounds in the literature and often a lack of clarity in how determinations were made, computational spectra and model compounds were used to support the interpretation of ECD and NMR spectra. A straightforward process to determine the configuration of these systems is presented.

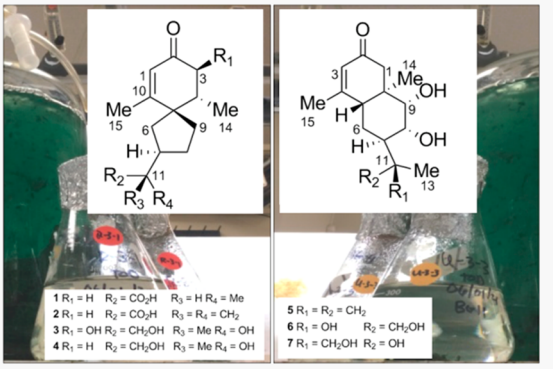

Cyanobacteria have been a rich source of biologically active secondary metabolites for the past 50 years.[1,2] Approximately 2000 species of cyanobacteria have been identified, with about 40 being toxigenic. Investigations into strains of these species have led to over 1600 natural products being reported from cyanobacteria alone. Studies illuminating the genetic diversity of cyanobacteria suggest they will remain an important source of new natural products for the foreseeable future.[1] Compounds isolated from cyanobacteria possess an extensive range of unique structural features and potential medical applications.[3] Interestingly, the vast majority of cyanobacterial compounds reported to date are intracellular metabolites with very little known about the types of metabolites excreted in the media at low concentrations.

As part of a larger study investigating polar metabolites produced in fermentation broths by strains within the extensive cyanobacterial collection at the University of Hawaii at Manoa, we have examined the media extracts of a *Calothrix* sp. (strain R-3-1) and a *Scytonema* sp. (strain U-3-3) that inhibited active transient receptor potential melastatin ion channels, e.g., TRPM7. TRPM7 contains an ion channel domain and a kinase domain that allow for the transport of calcium, magnesium, and other divalent ions and are essential for cell viability.[4] The cultures were grown from cryogenic storage to a 20 L scale in BG-11 media. It should be noted that while every attempt was made to grow the cyanobacterial cultures axenically, it is likely that the cultures were complex assemblages of organisms, as we have seen previously.[5] After approximately 45 days of culturing at the 20 L scale, the cell mass was separated from the media by filtration for later analysis, and HP20 resin was then added to the media for adsorption of secreted metabolites. After overnight agitation by aeration of the media, the HP20 resin was collected by filtration, lyophilized, and then exhaustively extracted in MeOH. The extract was then subjected to SPE followed by HPLC to isolate the extracted secondary metabolites. HPLC-UV-LCMS-guided isolation led to the discovery of seven sesquiterpenoid compounds, with six new and one known. Spironostoic acid (**1**), 11,12-didehydrospironostoic acid (**2**), and 12-hydroxy-2-oxo-11-*epi*-hinesol (**4**) are spirovetivane-type compounds, while stigolone (**5**), 11*R*,12-dihydroxystigolone (**6**), and 11*S*,12-dihydroxystigolone (**7**) are three eudesmane-type compounds primarily isolated from fungi. Interestingly, the literature shows considerable configurational

Received: October 26, 2021
Published: February 10, 2022

variation in the structure of spirovetivane-type compounds,[6−14] so in order to evaluate the variation in these deceptively simple molecules, we developed the following comprehensive approach based on analogous compounds and previous work in the literature while ignoring the isopropyl/isopropenyl tail for simplicity.

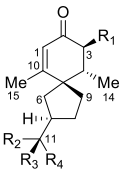

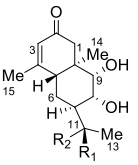

1 R_1 = H R_2 = CO_2H R_3 = H R_4 = Me
2 R_1 = H R_2 = CO_2H R_3 = R_4 = CH_2
3 R_1 = OH R_2 = CH_2OH R_3 = Me R_4 = OH
4 R_1 = H R_2 = CH_2OH R_3 = Me R_4 = OH

5 R_1 = R_2 = CH_2
6 R_1 = OH R_2 = CH_2OH
7 R_1 = CH_2OH R_2 = OH

RESULTS AND DISCUSSION

The structures of **1**−**7** were elucidated using a suite of spectroscopic and spectrometric techniques, such as LC-MS, ECD, and 1D and 2D NMR-based experiments. Compounds **1**−**4** were spirovetivane-type, while compounds **5**−**7** were all new eudesmane-type sesquiterpenoids. This paper represents the first report of **1**, **2**, and **4**−**7**, although **2** has been previously characterized as the methyl ester.[15] The spectroscopic properties of **3** show good agreement with previously reported data.[7,16,17] 2-(1′,2′-Dihydroxy-1′-methylethyl)-6,10-dimethyl-9-hydroxyspiro-[4,5]-dec-6-en-8-one (**3**) has previously been isolated several times with the earliest from potato tubers (*Solanum tuberosum*) infected with the fungus *Phoma exigua*.[7] Compound **4** is epimeric at C-11 to 2-oxo-12-hydroxyhinesol, previously described from a marine fungus, whose absolute configuration was determined by X-ray crystallography and ECD spectroscopy.[13]

The molecular formula of **1** was determined by HRESIMS to be $C_{15}H_{22}O_3$ based on the identification of a protonated molecule at m/z 251.1627 $[M + H]^+$ and sodium adduct ion at m/z 273.1463 $[M + Na]^+$. This molecular formula was consistent with the 15 carbon resonances present in the ^{13}C NMR spectrum and the number of oxygens suggested by analysis of the ^1H (Table 1) and ^{13}C spectra (Table 2).

Table 2. ^{13}C NMR Spectroscopic Data for Compounds 1−4 (δ in ppm)

no.[a]	**1**[b] (150 MHz)	**2**[b] (125 MHz)	**3**[b] (150 MHz)	**4**[c] (150 MHz)
1	126.2, CH	126.2, CH	123.1, CH	125.9, CH
2	202.2, C	202.2, C	201.4, C	199.3, C
3	43.5, CH_2	43.6, CH_2	75.7, CH	42.7, CH_2
4	38.6, CH	39.0, CH	47.3, CH	37.0, CH
5	51.8, C	51.8, C	52.2, C	49.8, C
6	36.2, CH_2	37.4, CH_2	32.0, CH_2	31.5, CH_2
7	45.1, CH	43.4, CH	48.8, CH	46.6, CH
8	32.9, CH_2	33.4, CH_2	28.8, CH_2	26.8, CH_2
9	35.9, CH_2	35.9, CH_2	36.9, CH_2	34.7, CH_2
10	172.2, C	172.4, C	173.3, C	168.1, C
11	49.8, CH	148.0, C	74.1, C	73.4, C
12	182.9, C	173.5, C	70.1, CH_2	69.6, CH_2
13	17.3, CH_3	119.9, CH_2	23.0, CH_3	22.1, CH_3
14	16.8, CH_3	16.8, CH_3	12.5, CH_3	16.4, CH_3
15	21.0, CH_3	21.0, CH_3	20.7, CH_3	20.7, CH_3

[a]Numbered consistent with ref 13. [b]MeOH-d_4. [c]$CDCl_3$.

Specifically, from the ^{13}C NMR spectrum, a carbonyl carbon could be identified at δ_C 202.2 (C-2) and a carboxyl at δ_C 182.9 (C-12), which combined required a total of three oxygen atoms. Analysis of IR data supported this conclusion via two carbonyl absorptions at 1666 and 1651 cm^{-1} and further clarified that the carboxyl group was a carboxylic acid, rather than an ester, based on a broad hydrogen-bonded OH signal present in the IR spectrum. These data also indicated that a third deshielded carbon resonance at δ_C 172.2 (C-10) was not

Table 1. ^1H NMR Spectroscopic Data for Compounds 1−4 (500 MHz, δ in ppm)

no.[a]	**1**[b]	(J in Hz)	**2**[b]	(J in Hz)	**3**[b]	(J in Hz)	**4**[c]	(J in Hz)
1	5.75	s	5.76	d (1.3)	5.72	d (1.3)	5.76	s
2								
3a	2.25	dd (16.9, 10.1)	2.26	dd (16.9, 10.4)	3.92	d (12.4)	2.21	dd (16.7, 9.9)
3b	2.43	dd (16.9, 4.3)	2.43	dd (16.9, 4.2)			2.43	dd (16.7, 4.2)
4	2.10	m	2.14	dd (10.4, 6.8)	1.89	m	2.10	m
5								
6a	1.23	dd (12.3, 12.3)	1.48	dd (12.5, 12.5)	1.48	m	1.49	dd (12.7, 12.7)
6b	2.08	m	2.21	m	2.08	dd (13.8, 7.6)	1.87	m
7	2.16	m	3.04	m	2.22	m	2.08	m
8a	1.50	dddd (12.1, 12.1, 9.6, 9.6)	1.72	dddd (11.5, 11.5, 9.7, 9.7)	1.71	m	1.72	m
8b	1.97	m	2.07	m	1.83	m	1.83	m
9a	1.86	m	1.95	m	1.80	m	1.82	m
9b	1.86	m	1.95	m	1.96	m	1.82	m
10								
11	2.20	m						
12a					3.38	d (10.9)	3.42	d (10.8)
12b					3.42	d (10.9)	3.54	d (10.8)
13a	1.16	d (6.8)	5.46	br s	1.18	s	1.20	s
13b			5.95	br s				
14	1.05	d (6.8)	1.09	d (6.8)	1.21	d (6.7)	1.01	d (6.9)
15	2.01	s	2.04	d (1.3)	2.04	d (1.3)	1.97	d (0.9)

[a]Numbered consistent with ref 13. [b]MeOH-d_4. [c]$CDCl_3$.

https://doi.org/10.1021/acs.jnatprod.1c01014
J. Nat. Prod. 2022, 85, 415−425

a carbonyl and instead part of a carbon−carbon double bond with the resonance at δ_C 126.2 (C-1) given the degrees of unsaturation. The deshielded shift of C-10 indicated that the double bond was conjugated to one of the carbonyls in an α,β-unsaturated system. Analysis of the 2D NMR data indicated that the sole olefinic proton signal at δ_H 5.75 (H-1) showed correlations to the ketone carbonyl at δ_C 202.2 (C-2), a methyl at δ_C 21.0 (C-15), a methylene at δ_C 43.5 (C-3), and a quaternary carbon at δ_C 51.8 (C-5). Further examination of the HMBC and COSY correlations around this fragment rapidly established a substituted cyclohexenone moiety; in particular, HMBC correlations from H_3-15 to C-1, C-5, and C-10 and then from H_3-14 to C-3, C-4, and C-5 were crucial in this assignment (Figure 1). Building on this ring, the spirocenter at C-5 was established by HMBC correlations to C-10 and C-4 from two sets of methylene protons (H_2-6 and H_2-9), which could be connected to each other via a series of COSY and HMBC correlations through C-7 and C-8 to form a five-membered ring. Appended at C-7 was the typical three-carbon branched unit found in the spirovetivanes, but, in the case of **1**, one of the typical methyl groups was oxidized to a carboxylic acid. Specific proton assignments were further verified and coupling constants extracted via analysis of DPFGSE-1D-TOCSY experiments.

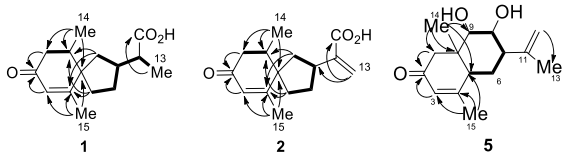

Figure 1. Key HMBC (arrow) and COSY (solid line) correlations used to determine the planar structures of **1**, **2**, and **5**.

At this point, when we attempted to assign the configuration of **1** by comparing its spectroscopic data with that of known compounds, the considerable configurational variation within this family of spirovetivane-type compounds[6−17] and the challenges in assigning the configuration became evident. As shown in the top half of Figure 2, there are four possible C-4/C-5 stereoisomers, each with two possible half-chair conformations to consider for the carbon core of the spirovetivane-type system. These stereoisomers differ in the orientation of the methyl group at C-14 of the cyclohexenone ring and their chair conformation. The conformations are designated HC($3\beta,4\alpha$) or HC($3\alpha,4\beta$), depending on whether C-3 or C-4 is above or below the plane of the alkene, with C-14 equatorial or axial.

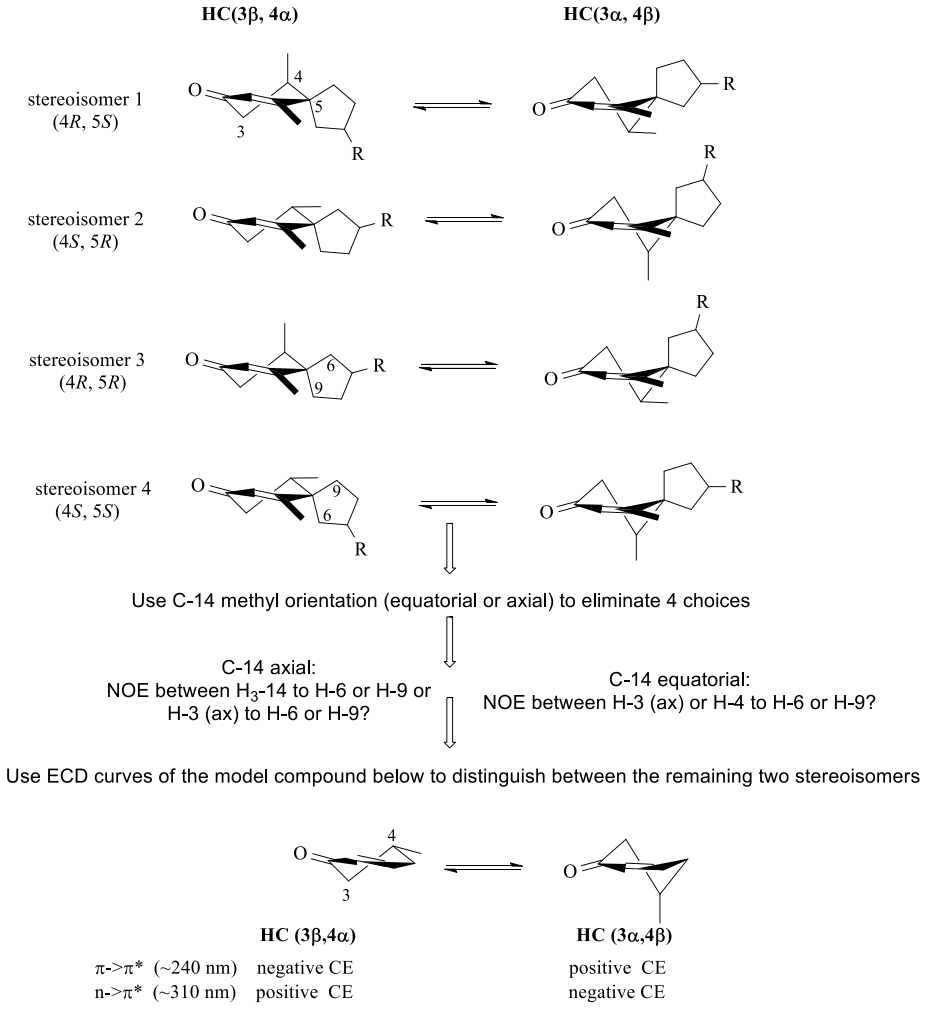

Figure 2. Possible stereoisomers and half-chair conformations of simplified spirovetivane-type compounds and the process for how to distinguish among them. Stereoisomers 1 and 2 are enantiomers, as are stereoisomers 3 and 4.

https://doi.org/10.1021/acs.jnatprod.1c01014
J. Nat. Prod. 2022, 85, 415−425

In terms of variation, from Figure 2 stereoisomer 1 HC(3β,4α),[6,9] stereoisomer 1 HC(3α,4β),[6,7,10,12] stereoisomer 3 HC(3β,4α),[7,8,11,14] and stereoisomer 4 HC(3β,4α)[13] have been reported for compounds of this type. Stereoisomer 4 HC(3α,4β) was only reported as part of a synthesis of (+)-β-vetivone,[8] and there were no reports of stereoisomer 2 from the literature reviewed. It was difficult to assess the conclusions on absolute configuration for many of the compounds by applying the approach in Figure 2, as there was often a lack of accessible data, such as ECD data. In addition, in some cases, the specific rotation was used to assign the absolute configuration at C-5, C-7, and C-11 by comparing with a previous publication, but we would urge caution going forward. The reported variety in configuration and the effects of conformation on such measurements for the spirovetivane-type compounds undermine the validity of that approach.

To assign the configuration of spirovetivane-type compounds (Figure 2), it is easiest to begin with the orientation of the methyl (C-14) attached to C-4 on the cyclohexanone ring. Depending on whether the C-14 methyl is in an axial or equatorial orientation, NOE cross-peaks from H-6 or H-9 to H_3-14 or that from H-3$_{ax}$ or H-4 can be used to assign the relative configuration of the spirocenter. In some cases, this can be challenging to assign with confidence due to the complexity and broadness of the signals, and additional NMR experiments might be required. Once the spriocenter is assigned, though, ECD data can then effectively distinguish between the two remaining structures, which should be enantiomers with regard to the spirovetivane core. Simple sector rules are not applicable here, as the cyclohexanone chromophore is not planar,[18,19] yet the conformation of the cyclohexanone system still determines the ECD Cotton effects. For example, 4*R*-methylcyclohex-2-enone exhibits two possible half-chair conformations as depicted in Figure 2 that yield opposite signs for Cotton effects at the $\pi \rightarrow \pi^*$ and n $\rightarrow \pi^*$ transitions.[18] In our spirovetivane-type system, a negative $\pi \rightarrow \pi^*$ and positive n $\rightarrow \pi^*$ would indicate HC(3β,4α). The only major caveat is that a substitution at C-6 or C-9 might interfere with the preferred half-chair conformation, so careful conformational analysis is critical due to the variation mentioned above. For this reason, a conformational analysis was performed to support the assertions in the paper following the procedure outlined in the Computational Methods section. These data allowed comparisons between relevant theoretical and experimental data (coupling constants, chemical shifts, etc.; vide infra), which was critical for understanding the spiro systems in particular (see Supporting Information Tables S7 and S8).

The relative and absolute configuration of **1** was established through the general approach outlined above. Analysis of coupling constants within the cyclohexenone moiety places H-3a and H-4 in an axial orientation based on a 10.0 Hz coupling between them, thereby placing CH_3-14 in an equatorial orientation. This value was in good agreement with our calculated values (calcd for 10.3 Hz by Karplus; Table S7). Because the C-14 methyl is equatorially oriented, a variety of NMR experiments were utilized to obtain well-resolved 1D NOE signals (Figure 3) between H-3$_{ax}$ (δ 2.25 dd J = 16.9, 10.1) to H-6b (calcd for average distance 2.31 Å; Table S8) and H-4 to H_2-9 (calcd for average distance 2.43 Å; Table S8), which established the relative configuration at spirocenter C-5, leaving stereoisomer 3 HC(3α,4β) and stereoisomer 4 HC(3β,4α) (Figure 2) as possibilities. The experimental ECD spectrum (Figure 4) showed a negative Cotton effect

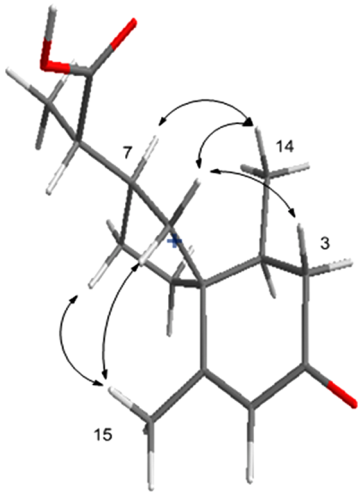

Figure 3. Key NOE correlations used to determine the relative configuration of **1**.

for $\pi \rightarrow \pi^*$ and positive for n $\rightarrow \pi^*$, indicating the spirovetivane core corresponded to stereoisomer 4 HC(3β,4α). This conclusion was supported by our configurational analysis, which indicated (3β,4α) is the preferred conformation (79.1% HC(3β,4α) with 14$_{eq}$ and 13.2% HC(3α,4β) with 14$_{ax}$; Table S7). Thus, the cyclohexenone core of **1** was similar to the previously characterized 2-oxo-12-hydroxyhinesol (**1**: $\Delta\varepsilon$ = −3.8 at 237 nm; lit.:[13] $\Delta\varepsilon$ = −3.30 at 239 nm), whose structure was established by X-ray crystallography.[13] Finally, the configuration of C-7, the last stereogenic center within the rings, was established via an NOE cross-peak between H-7 and H_3-14.

Unfortunately, no clear configurational assignment could be made from the available spectroscopic data for the remaining stereogenic center C-11 outside the rings. However, our computational NMR data supported an 11*S* configuration with a DP4+ probability for scaled and unscaled data calculated at 97.9%, suggesting the final assignment of **1** to be 4*S*, 5*S*, 7*R*, 11*S*. The absolute configuration was supported by TDDFT[20,21] calculations conducted at the BHandHLYP/def2tzvpp level, which predicted ECD data with a similarity factor of 0.8175 (σ = 0.3 eV; shift = 18 nm) as calculated by SpecDis[22] when compared to our experimental data (Figure S20).

Compound **2**, which was previously isolated as the methyl ester from *Cassinia subtropica*,[15] had a molecular formula of $C_{15}H_{20}O_3$ based on HRESIMS identification of a protonated molecule at m/z 249.1472 $[M + H]^+$ and sodium adduct ion at m/z 271.1306 $[M + Na]^+$. Similarities between the ^{1}H and ^{13}C NMR spectra indicated that **2** was structurally similar to **1**, but two atomic mass units smaller. The most striking difference in the ^{1}H NMR spectrum was the absence of a third methyl resonance at δ_H 1.17 (H-17) and the presence of two additional deshielded olefinic protons at δ_H 5.46 (H-13a) and δ_H 5.95 (H-13b). The location of this new terminal alkene was established based on HMBC correlations between these vinyl protons and C-7, C-11, and C-12. The relative and absolute configurations of **2** were established following the process in Figure 2 as 4*S*, 5*S*, 7*R*, based on the C-14 equatorial methyl group, the NOE correlations observed in Figure 5, and the ECD spectrum shown in Figure 4.

A sodium adduct ion at m/z 291.1586 $[M + Na]^+$ from HRESIMS established that **3** had a molecular formula of

https://doi.org/10.1021/acs.jnatprod.1c01014
J. Nat. Prod. 2022, 85, 415−425

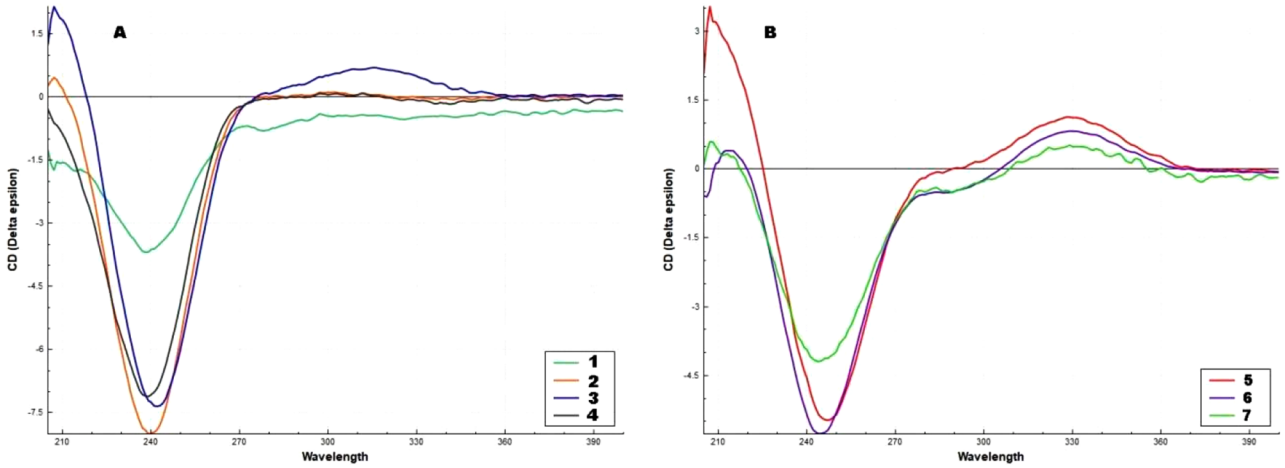

Figure 4. Experimental ECD spectra of **1**−**4** (A) and **5**−**7** (B).

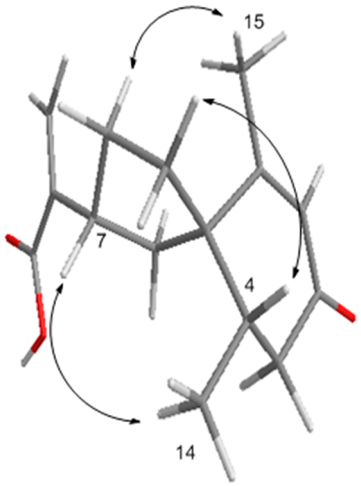

Figure 5. Key NOE correlations used to determine the relative configuration of **2**.

$C_{15}H_{24}O_4$. Spectral similarities to **1** and **2** were evident with major differences being the loss of the carboxyl resonance at C-12 and the addition of three oxygenated carbon signals in the ^{13}C NMR spectrum (δ_C 75.7, C-3; δ_C 74.1, C-11; δ_C 70.1, C-12) and three signals in the ^1H NMR spectrum (δ_H 3.38, H-12a; δ_H 3.42, H-12b; δ_H 3.92, H-3). The rest of the spiroskeleton was confirmed through 2D NMR analysis, which yielded the structure of **3** with the three hydroxy groups at C-3, C-11, and C-12, corresponding to a planar structure previously reported.[7,16,17] Given the configurational variability noted before, the relative and absolute configuration of **3** was determined according to Figure 2 as 3*S*, 4*R*, 5*S*, and 7*R* (J = 12.4 Hz for H-3a to H-4 establishing equatorial C-14, NOE between H-3a and H-6b, negative Cotton effect at 243 nm). Again, for C-11, experimental and computational scaled and unscaled NMR data were compared using DP4+ to distinguish between 11*R* and 11*S* with support (96.7%) for the 11*S* configuration. A similarity factor of 0.9089 (σ = 0.3 eV; shift = 18 nm) was calculated by Specdis for comparison of calculated and experimental ECD curves in MeOH for (3*S*,4*R*,5*S*,7*R*,11*S*)-**3** (Figure S46).

Compound **4** was initially thought to be the same as 2-oxo-12-hydroxyhinesol isolated from *Atractylodes lancea* fermented by a marine fungus[13] based on all spectroscopic data. However, upon closer inspection, the NMR data of **4** differ significantly from that compound at C-6, C-9, and their associated protons. The same approach as with the three previous compounds was employed to establish the core carbon skeleton as 4*S*, 5*S*, and 7*R*, matching 2-oxo-12-hydroxyhinesol, which showed the differences were attributed to the three-carbon tail. The combination of scaled and unscaled NMR data for DP4+ analysis indicates **4** is likely 11*S* with 80.3% probability of "modest confidence" (90% > x > 50%),[23] so the final absolute assignment is 4*S*, 5*S*, 7*R*, 11*S*, epimeric at C-11 to 2-oxo-12-hydroxyhinesol.[13] These assignments are further supported by CP3 analysis, which compares experimental NMR data for two diastereomers with calculated data. CP3 analysis using ^{13}C and ^1H NMR data also suggests that the compound isolated in this study has an 11*S* configuration (100% probability) and the previously isolated epimer has an 11*R* absolute configuration. The SpecDis similarity factor was 0.9640 (σ = 0.3 eV; shift = 19 nm) for comparison of calculated and experimental ECD curves of **4** (Figure S60).

Compound **5**, the first eudesmane-type sesquiterpenoid isolated, had a molecular formula of $C_{15}H_{22}O_3$ based on the identification of a protonated molecule and a sodium adduct ion at m/z 251.1639 $[M + H]^+$ and at m/z 273.1460 $[M + Na]^+$, respectively. Initially, the similarities between the ^1H (Table 3) and ^{13}C (Table 4) NMR and MS spectra of **5** and **1** suggested a spirovetivane-type structure. However, upon closer inspection of all of the data, differences became apparent, indicating the carbon skeleton was not the same. A substituted cyclohexenone fragment was rapidly assembled based on HMBC correlations from H_3-14 and H_3-15, but, unlike in the case of **1**, H_2-6 and H-9 both did not show HMBC correlations to C-10 and C-4, indicating **5** lacked the spirocenter. Instead, H_3-14 showed an HMBC correlation to C-5, suggestive of a decalin system, and displayed a small coupling (1.2 Hz) typically observed between the methyl group of a *trans*-decalin system and axial protons.[24] Other new signals apparent in the ^1H NMR spectrum were consistent with a terminal olefin (δ_H 4.85, H-12a, δ_H 5.02, H-12b) and oxidation at C-8 (δ_H 4.20, H-8) and C-9 (δ_H 3.55, H-9) to hydroxy groups, facts corroborated by the broad IR absorption at 3418 cm^{-1} and the 2D NMR data.

The relative configuration of **5** was determined by analyses of relevant NOE correlations (Figure 6) and coupling constants and supported by conformational analysis (Tables

https://doi.org/10.1021/acs.jnatprod.1c01014
J. Nat. Prod. 2022, 85, 415−425

Table 3. ^{1}H NMR Spectroscopic Data for Compounds 5−7 in MeOH-d_4 (500 MHz, δ in ppm)

no.	5	(J in Hz)	6	(J in Hz)	7	(J in Hz)
1a	2.11	m	2.13	d (16.1)	2.15	dd (16.2, 1.3)
1b	2.63	d (15.8)	2.63	d (16.1)	2.63	d (16.2)
2						
3	5.86	m	5.82	br s	5.84	br s
4						
5	2.56	ddd (13.3, 2.8, 1.4)	3.12	d (13.6)	3.04	d (13.5)
6a	1.94	td (13.3, 5.5)	1.74	dt (13.6, 7.1)	1.80	td (13.5, 6.3)
6b	2.08	m	2.18	d (14.5)	2.09	d (14.1)
7	2.60	m	2.00	m	2.04	m
8	4.20	dt (3.3, 1.6)	4.17	d (4.0)	4.14	m
9	3.55	d (3.3)	3.86	d (4.0)	3.87	d (4.1)
10						
11						
12a	4.85	m	3.44	d (10.9)	3.44	d (10.9)
12b	5.02	d (1.4)	3.61	d (10.9)	3.51	d (10.9)
13	1.85	dt (1.4, 0.7)	1.33	s	1.29	s
14	1.07	d (1.1)	1.04	br s	1.04	d (1.3)
15	2.00	t (1.4)	2.01	t (1.4)	2.02	t (1.4)

Table 4. ^{13}C NMR Spectroscopic Data for Compounds 5−7 MeOH-d_4 (δ in ppm)

no.	5 (125 MHz)	6[a]	7 (150 MHz)
1	52.5, CH_2	52.4, CH_2	52.6, CH_2
2	202.1, C	202.5, C	202.3, C
3	127.1, CH	126.5, CH	126.7, CH
4	166.3, C	167.6, C	167.0, C
5	43.6, CH	43.9, CH	44.3, CH
6	21.3, CH_2	19.8, CH_2	20.4, CH_2
7	47.7, CH	46.5, CH	45.5, CH
8	72.5, CH	71.7, CH	71.4, CH
9	75.8, CH	76.9, CH	76.9, CH
10	44.6, C	43.5, C	43.7, C
11	145.9, C	74.9, C	75.2, C
12	112.6, CH_2	69.3, CH_2	69.5, CH_2
13	23.5, CH_3	25.5, CH_3	24.5, CH_3
14	13.2, CH_3	12.8, CH_3	13.0, CH_3
15	22.6, CH_3	22.5, CH_3	22.7, CH_3

[a]All C signals for compound 6 from HSQC/HMBC.

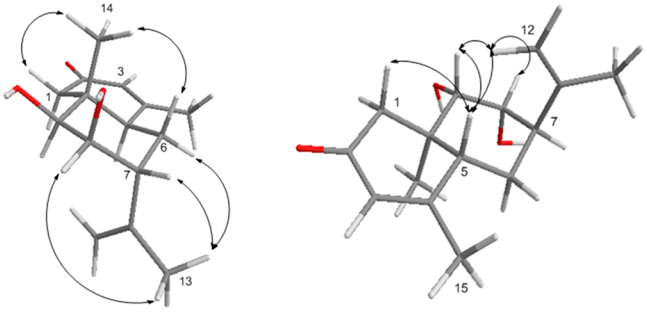

Figure 6. Key NOE correlations used to determine the relative configuration of 5.

S7 and S8). In particular, a strong NOE correlation from H_3-14 to H-6a established their axial positions given the $^3J_{H,H}$ value of 13.3 Hz between H-6a and bridgehead proton H-5, while NOE correlations from H-5 to H-1a (calcd average distance 2.45 Å) and to H-9 (calcd average distance 2.43 Å) placed those protons in an axial orientation on the opposite face of the decalin system. A strong NOE correlation from H-5 to H-12a (calcd average distance 3.53 Å)[25] indicated an axial position for the isopropenyl tail, not unprecedented among eudesmane-type compounds.[26,27] This axial assignment is further supported by a lack of correlation from H-7 to H-5 and small coupling constants for H-8 and H-6a to H-7. Computational analysis of the conformations of 5 suggests that the lowest energy conformers do indeed have the isopropenyl unit in an axial orientation. This conformation is 2.5 kcal/mol lower in energy than the lowest energy conformer with equatorial orientation. Finally, an NOE correlation between H-9 and H-8, along with $^3J_{H,H}$ value of 3.3 Hz (calcd for 3.6 Hz by Karplus) between these two protons, established the equatorial orientation of H-8.

The absolute configuration was determined by ECD in comparison to literature values. Once again, there is considerable configurational variation and a lack of clarity about how some of those assignments were made for the eudesmane-type systems,[26−35] leading us to articulate our approach in some detail. For a *trans*-decalin system (*cis* not considered), there are four possible half-chair conformations with two designated HC(1α,10β) and two HC(1β,10α) when the orientations of the hydroxy groups and the isopropenyl tail are ignored for simplicity (Figure 7). ECD data for steroidal structures analogous to the four diastereomers were used for comparison, and as stated previously, ECD curves are determined by the helicity of the enone. This analysis indicated that the common steroids (6*t*3 class) followed the same ECD pattern observed for 1−4. However, those analogous to 5 belonging to the 6*t*4 class (Figure 8) followed opposite rules for ECD curves (Figure 7).[36] The main caveat is that a π-donor γ-axial to the α,β-unsaturated ketone can affect and likely reverse the expected signs for the ECD Cotton curves, but this is not the case with 5.[36] With the isopropenyl tail pseudoaxial, the positive n−π* and negative π−π* Cotton effects indicate 5 corresponds to diastereomer 2 in Figure 7, i.e., 5*R*, 7*R*, 8*R*, 9*S*, 10*R*, taking into account the previously elucidated relative configuration. Conformational analysis also supported this conclusion, as almost 98% of all conformers, with a population greater than one mole percent, are HC(1α,10β) with C-14 Me axial. Calculated and experimental ECD spectra show good agreement, with a similarity factor of 0.9636 (σ = 0.3 eV; shift = 14 nm) for (5*R*,7*R*,8*R*,9*S*,10*R*)-5 (Figure S81).

Compounds 6 and 7 were also eudesmane-type sesquiterpenoids. HRMS provided a molecular formula of $C_{15}H_{24}O_5$ for both compounds corresponding to two additional hydroxy groups in each compared to 5. The main differences in the ^{1}H NMR spectrum (Table 3) in relation to 5 were the terminal olefin signals being replaced with resonances corresponding to an oxygenated methylene. Unfortunately, because of the amount of 6 available, ^{13}C NMR resonances needed to be extracted from HSQC and HMBC data sets. From the ^{13}C signals (Table 4), it was also clear that C-11 and C-12 were both oxygenated (6: δ_C 74.8, C-11 and δ_C 69.2, C-12; 7: δ_C 75.2, C-11 and δ_C 69.5 (C-12), and with no other apparent spectral difference between 6 and 7, these compounds must be epimeric at C-11. While the relative configuration of the remaining stereogenic centers in 6 and 7 could be established in the same manner as with 5 through key NOESY correlations

https://doi.org/10.1021/acs.jnatprod.1c01014
J. Nat. Prod. 2022, 85, 415−425

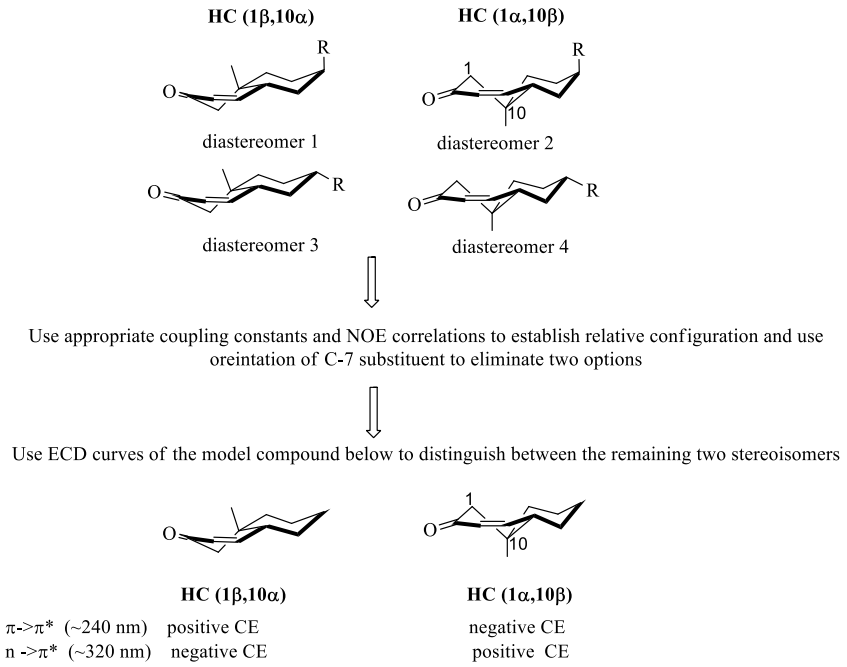

Figure 7. Procedure for assigning the configuration of simplified *trans*-decalin eudesmane-type compounds with the half-chair conformations.

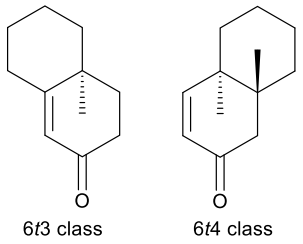

Figure 8. Two types of steroid class with 6*t*3 observed in common steroids and 6*t*4 being analogous to **5**−**7**.

(H-5 to H-1a, H-6b, H-9, and H-12a/b or H_3-13; H_3-14 to H-6a and H-1b, H-9 to H-8) supported by conformational analysis of interatomic distances (Table S8), due to rotation of the C-7 to C-11 bond, it was impossible to decide definitively for C-11 based on a comparison of the NOESY spectra alone. Combining our NOE and molecular modeling data suggested some signals that can help differentiate them, however. For **6**, if the OH at C-11 is positioned over the structure (Figure 9), then the strong NOE signals from H_3-13 to H-8 and to H-9 and from H-12a/b to H-5 and to H-6b indicate a likely 11*R* configuration. This conclusion is supported by the conformational analysis of those conformers with greater than 1 mole percent (80.6% of Boltzmann population), where the C-11 OH was positioned over the decalin system for 79.3% of the Boltzmann population, corresponding to all but one (1.3%) of the conformers analyzed. Observation of this NOE helped to establish the configuration of C-11 as 11*R*. For **7**, if the OH at C-11 is positioned over the structure (Figure 9), then the strong NOE signals from H_3-13 to H-6b and H-12a/b to H-8 would indicate 11*S*. Molecular modeling data indicate 85.2 mole percent of the lowest energy conformers would show an NOE between H-5 and H_3-13 and have the C-11 hydroxy group positioned over the decalin system, which established the configuration as 11*S*. CP3 calculations comparing the experimental to calculated NMR spectra support that **6** is 11*R*, while **7** is 11*S* with a 97% probability for ^{1}H alone and 100% when both ^{13}C and ^{1}H data are taken into account, although some of the ^{13}C NMR shifts are taken from 2D data. Based on this, compound **6** is presented as 5*R*, 7*S*, 8*R*, 9*S*, 10*R*, 11*R* and **7** as 5*R*, 7*S*, 8*R*, 9*S*, 10*R*, 11*S* with SpecDis similarity factors of 0.8335 (σ = 0.3 eV; shift = 14 nm) and 0.8534 (σ = 0.3 eV; shift = 12 nm) for comparison of calculated and experimental ECD, respectively (Figures S93 and S102).

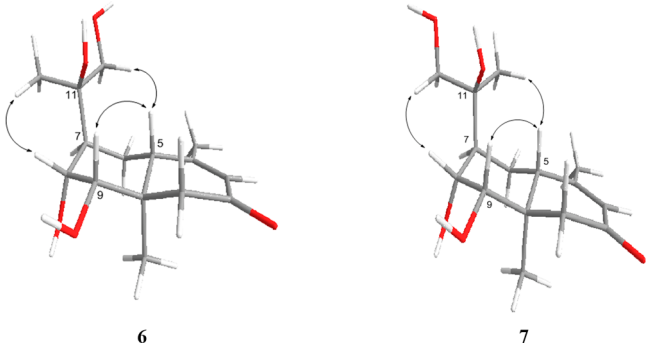

Figure 9. Key NOE correlations used to determine the relative configuration of **6** and **7**.

As mentioned earlier, the original extracts were tested against a series of TRPM ion channels in a high-throughput fluorescent screen and led to the isolation work described herein. Subsequent retesting of the media extract of R-3-1 (Figure S110) in a patch-clamp assay failed to reproduce the inhibitory effect observed against TRPM7. At the same time, the media extract of U-3-3 (Figure S110) also showed no difference from controls in the secondary patch-clamp assay for TRPM2. When the purified compounds were tested, they were essentially inactive. For example, **2** displayed only slight inhibition of TRPM7 at 50 μM, and **7** displayed 76% inhibition at 44 μM to TRPM2 with only minor inhibition at 10 μM (Figure S111).

https://doi.org/10.1021/acs.jnatprod.1c01014
J. Nat. Prod. 2022, 85, 415−425

CONCLUSION

In conclusion, the sesquiterpenoid compounds isolated (**1**−**7**) showed little activity in the TRPM assays. Still, these deceptively simple molecules proved to be a surprising challenge regarding their structure elucidation, partially due to the reported variation in the literature, often with few details in how determinations of the relative and absolute configurations were made. This challenge offered an opportunity to build a comprehensive approach to solving the absolute configuration for structures of both spirovetivane- (Figure 2) and eudesmane-type (Figure 7) compounds using common spectroscopic approaches, chiefly NMR and ECD. Computational techniques were integral in supporting the proposed approaches by providing a better understanding of accessible conformational space for diastereomers and their chemical shift differences. We hope this paper will help ease the consternation of the researchers who isolate new spirovetivane- and eudesmane-type compounds, which are prevalent throughout the literature, by providing a straightforward approach to their structure determination.

EXPERIMENTAL SECTION

General Experimental Procedures. Optical rotation measurements were taken on a JASCO DIP-370 digital polarimeter at the sodium line (589 nm). UV spectra were obtained on a Varian Cary 50 Bio UV−vis spectrophotometer with a quartz cuvette in methanol. ECD measurements were taken on a Chirascan circular dichroism spectrometer with the sample dissolved in MeOH and placed in a 1 cm quartz cuvette with a solvent subtraction for baseline correction. IR spectra were recorded on a CaF_2 salt plate using a Shimadzu IRAffinity-1 Fourier-transform infrared spectrophotometer. All NMR spectra for compounds were acquired on a Varian Unity Inova 500 MHz spectrometer operating at 500 MHz for ^{1}H or 125 MHz for ^{13}C or an Agilent Technologies 600 MHz DD2 spectrometer operating at 599.58 MHz for ^{1}H and 150.78 MHz for ^{13}C NMR. The appropriate residual solvent signal was used as an internal reference (^{1}H: 7.26 for $CDCl_3$, 3.31 for MeOH-d_4; ^{13}C: 77.0 for $CDCl_3$, 49.0 for MeOH-d_4). All NMR samples were placed in 3 mm Shigemi tubes for analysis. An Agilent 6545 LC-MS Q-Tof with ESI ionization was used in the positive mode to acquire HRMS data with a C18 Agilent Eclipse Plus (1.8 μm, 2.1 × 50 mm) column. HPLC separations were performed using a Shimadzu system consisting of an LC-20AB binary, high-pressure gradient solvent delivery unit, an SPD-M20A photodiode array detector, and a CBM-20A system controller. BG-11 media formulation was composed of the following: $NaNO_3$ 1.5 g/L, $K_2HPO_4{\cdot}3H_2O$ 0.04 g/L, $MgSO_4{\cdot}7H_2O$ 0.075 g/L, Na_2CO_3 0.02 g/L, $CaCl_2{\cdot}2H_2O$ 0.036 g/L, Na_2EDTA 0.001 g/L, ferric ammonium citrate 0.006 g/L, and citric acid 0.006 g/L with trace metals H_3BO_3 2.86 mg/L, $MnCl_2{\cdot}4H_2O$ 1.81 mg/L, $ZnSO_4{\cdot}7H_2O$ 0.22 mg/L, $Na_2MoO_4{\cdot}2H_2O$ 0.39 mg/L, $CuSO_4{\cdot}5H_2O$ 0.08 mg/L, and $Co(NO_3)_2{\cdot}6H_2O$ 0.05 mg/L.

Collection and Identification. The sample designated R-3-1 was collected in Foster Botanical Garden (21 19.00 N, 157 51.30 W) on Oahu from a freshwater stream. The sample was identified as *Calothrix* sp. by Dr. Charles O'Kelly. It possessed tapered trichomes that were mostly straight and 8−15 μm in diameter at the base while tapering to 3−5 μm at the tips. It possessed basal heterocysts and occasional false branching identical to other strains in our collection that had been identified by 16s RNA sequencing as *Calothrix* sp. The other strain used in this study, U-3-3, was collected from Majuro Atoll, Marshall Islands (7 10.00 N, 171 12.00 E) and previously identified by 16 sRNA sequencing as *Scytonema* sp. (GenBank accession number AY069954).

Fermentation and Isolation of Compounds. Both cyanobacterial strains, R-3-1 (*Calothrix* sp.) and U-3-3 (*Scytonema* sp.), were revived from cryogenic storage, grown in BG-11 media, and scaled up to 20 L. The cultures were grown aerated at a flow rate of 4−5 L/min under continuous illumination of fluorescent light. The cell mass was removed from the media after 45 days by filtration, and the resulting biomass was freeze-dried. HP20 resin was added to the media, and after 24 h of mixing by aeration, the HP20 resin was collected by filtration. The resin was then placed in a −80 °C freezer overnight and lyophilized. The lyophilized HP20 beads (U-3-3: 80.46 g; R-3-1: 104.06 g) were exhaustively extracted in MeOH (U-3-3: 1 × 750 mL and 2 × 500 mL; R-3-1: 1 × 850 mL and 2 × 500 mL) with shaking for 12 h. The combined organic extract from each growth was evaporated to dryness, yielding brownish residues (U-3-3: 235.0 mg; R-3-1: 162.0 mg). The residues were reconstituted in MeOH (1.5 mL), sonicated, and fractionated over C8 silica gel eluting with increasing amounts of MeOH in H_2O (R-3-1: 25%, 75%, 90%, and 100% MeOH; U-3-3: 25%, 50%, 75%, and 100% MeOH).

The 75% MeOH fraction (59.8 mg of dried residue) of R-3-1 was separated using a Phenomenex Luna C18 semipreparative column (250 × 10 mm, 5 μm; PDA detection, flow rate: 2.7 mL/min) with a gradient of 5% CH_3CN in H_2O (0.1% formic acid in each) for 2 min, then a linear gradient from 5% to 70% over 20 min, before increasing to 100% over 2 min and washing with 100% CH_3CN for 10 min with a PDA detector. The order of elution for compounds **1**−**4** was **4** (t_R = 16.7−18.3 min), **1** (t_R = 21.5−22.5 min), and **2** and **3** (t_R = 22.5−23.5 min). These compounds were subsequently purified by HPLC using a Phenomenex Luna PFP semipreparative column (250 × 10 mm, 5 μm, PDA detection, flow rate: 2.7 mL/min) eluting with increasing amounts of MeOH in H_2O with 0.1% formic acid. Compound **4** (t_R = 11.0 min, 2.6 mg, 1.60% yield, 94.0% pure by UV at 240 nm) was purified using a linear gradient of 60% to 80% over 25 min. A linear gradient of 65% to 85% MeOH in H_2O over 25 min was used to purify **1** (t_R = 14.0 min, 0.7 mg, 0.43% yield, 98.6% pure by UV at 240 nm), **2** (t_R = 15.0 min, 1.0 mg, 0.62% yield, 97.5% pure by UV at 240 nm), and **3** (t_R = 7.2 min, 0.8 mg, 0.49% yield, 99.4% pure by UV at 240 nm).

The 50% MeOH fraction (27.0 mg of dried residue) of U-3-3 yielded **6** and **7** after HPLC purification. This fraction was separated using a Phenomenex Luna C18 semipreparative column (250 × 10 mm, 5 μm, PDA detection, flow rate: 2.7 mL/min) using a linear gradient from 20% to 70% CH_3CN and H_2O (0.1% formic acid in each) after an initial 2 min at 20%. The fraction collected between 14.9 and 16.1 min was then separated on a Phenomenex Luna PFP semipreparative column (250 × 10 mm, 5 μm, flow rate: 2.1 mL/min) using a linear gradient of 50−100% over 20 min after a 2 min initial hold at 50% to yield **6** (t_R = 10.3 min, 1.1 mg, 0.47% yield, 82.2% pure by UV at 240 nm) and **7** (t_R = 12.3 min, 0.4 mg, 0.17% yield, 72.3% pure by UV at 240 nm).

The 75% fraction of U-3-3 (11.6 mg of dried residue) provided compound **5**. Using a two-step purification procedure similar to **6**, the 75% MeOH fraction was first purified on a Phenomenex Luna C18 semipreparative column (linear gradient 20−75% over 20 min; flow rate: 2.7 mL/min), and the eluant collected between 16.8 and 17.9 min was repurified on a Phenomenex Luna PFP semipreparative column (linear gradient of 50−85% over 30 min; flow rate: 2.7 mL/min) to yield **5** (t_R = 18.2 min, 1.4 mg, 0.60% yield, 100.0% pure by UV at 240 nm).

*Spironostoic Acid (**1**).* White solid; $[\alpha]_D^{21}$ −88 (*c* 0.1, MeOH); UV (MeOH) λ_{max} (log ε) 237 (4.00) nm; ECD (*c* 0.1 MeOH) λ_{max} ($\Delta\varepsilon$) 237 (−3.8) nm; IR (CaF_2 disc) ν_{max} 3442, 2959, 1666, 1651, 1573 cm^{-1}; ^{1}H and ^{13}C NMR data, Tables 1 and 2; HRESIMS *m*/*z* 251.1627 $[M + H]^+$ (calcd for $C_{15}H_{23}O_3$ (+1), 251.1642); 273.1463 $[M + Na]^+$ (calcd for $C_{15}H_{22}O_3Na$ (+1), 273.1461).

*11,12-Didehydrospironostoic Acid (**2**).* White solid; $[\alpha]_D^{21}$ −82 (*c* 0.1, MeOH); UV (MeOH) λ_{max} (log ε) 240 (4.16) nm; ECD (*c* 0.1 MeOH) λ_{max} ($\Delta\varepsilon$) 241 (−8.0) nm; IR (CaF_2 disc) ν_{max} 3470, 2958, 2875, 1655 cm^{-1}; ^{1}H and ^{13}C NMR data, Tables 1 and 2; HRESIMS *m*/*z* 249.1472 $[M + H]^+$ (calcd for $C_{15}H_{21}O_3$ (+1) 249.1485); 271.1306 $[M + Na]^+$ (calcd for $C_{15}H_{20}O_3Na$ (+1), 271.1305).

*2-(1′,2′-Dihydroxy-1′-methylethyl)-6,10-dimethyl-9-hydroxy-spiro-[4,5]-dec-6-en-8-one (**3**).* White solid; $[\alpha]_D^{21}$ −51 (*c* 0.1, MeOH); UV (MeOH) λ_{max} (log ε) 241 (4.08) nm; ECD (*c* 0.1 MeOH) λ_{max} ($\Delta\varepsilon$) 243 (−7.4) nm; IR (CaF_2 disc) ν_{max} 3400, 2922,

https://doi.org/10.1021/acs.jnatprod.1c01014
J. Nat. Prod. 2022, 85, 415−425

2851, 1591 cm^{-1}; ^1H and ^{13}C NMR data, Tables 1 and 2; HRESIMS *m/z* 269.1766 $[M + H]^+$ (calcd for $C_{15}H_{25}O_4$ (+1) 269.1747); 291.1586 $[M + Na]^+$ (calcd for $C_{15}H_{24}O_4Na$ (+1) 291.1567); 559.3250 $[2\ M + Na]^+$ (calcd for $C_{30}H_{48}O_8Na$ (+1) 559.3241).

*12-Hydroxy-2-oxo-11-epi-hinesol (**4**).* White solid; $[\alpha]_D^{21}$ −111 (*c* 0.1, MeOH); UV (MeOH) λ_{max} (log ε) 240 (4.02) nm; ECD (*c* 0.1 MeOH) λ_{max} ($\Delta\varepsilon$) 239 (−7.1) nm; IR (CaF_2 disc) ν_{max} 3417, 2879, 1651 cm^{-1}; ^1H and ^{13}C NMR data, Tables 1 and 2; HRESIMS *m/z* 253.1806 [M + H]+ (calcd for $C_{15}H_{25}O_3$ (+1) 253.1798); 275.1615 $[M + Na]^+$ (calcd for $C_{15}H_{24}O_3Na$ (+1) 253.1798); 235.1695 $(M + H)^+[-H_2O]$ (calcd for $C_{15}H_{23}O_2$ (+1) 235.1693).

*Stigolone (**5**).* White solid; $[\alpha]_D^{21}$ +51 (*c* 0.1, MeOH); UV (MeOH) λ_{max} (log ε) 240 (4.03) nm; ECD (*c* 0.1 MeOH) λ_{max} ($\Delta\varepsilon$) 327 (+1.1), 248 (−5.5) nm; IR (CaF_2 disc) ν_{max} 3418, 2968, 2920, 1660, 1645 cm^{-1}; ^1H and ^{13}C NMR data, Tables 3 and 4; HRESIMS *m/z* 251.1639 $[M + H]^+$ (calcd for $C_{15}H_{23}O_3$ (+1) 251.1642); 273.1460 $[M + Na]^+$ (calcd for $C_{15}H_{22}O_3Na$ (+1) 273.1461); 523.3028 $[2\ M + Na]^+$ (calcd for $C_{30}H_{44}O_6Na$ (+1) 523.3030).

*11R,12-Dihydroxystigolone (**6**).* White solid; $[\alpha]_D^{21}$ +22 (*c* 0.1, MeOH); UV (MeOH) λ_{max} (log ε) 235 (4.29) nm; ECD (*c* 0.1 MeOH) λ_{max} ($\Delta\varepsilon$) 331 (+0.8), 246 (−5.8) nm; IR (CaF_2 disc) ν_{max} 3375, 2964, 2922, 2854, 1651, 1654 cm^{-1}; ^1H and ^{13}C NMR data, Tables 3 and 4; HRESIMS *m/z* 285.1696 $[M + H]^+$ (calcd for $C_{15}H_{25}O_5$ (+1) 285.1697); 307.1516 $[M + Na]^+$ (calcd for $C_{15}H_{24}O_5Na$ (+1) 307.1516); 323.1242 $[M + K]^+$ (calcd for $C_{15}H_{24}O_5K$ (+1) 323.1255); 267.1587 $(M + H)^+[-H_2O]$ (calcd for $C_{15}H_{23}O_4$ (+1) 267.1591).

*11S,12-Dihydroxystigolone (**7**).* White solid; $[\alpha]_D^{21}$ +20 (*c* 0.1, MeOH); UV (MeOH) λ_{max} (log ε) 235 (4.14) nm; ECD (*c* 0.1 MeOH) λ_{max} ($\Delta\varepsilon$) 331 (+0.6), 243 (−4.3) nm; IR (CaF_2 disc) ν_{max} 3410, 2924, 2820, 1591 cm^{-1}; ^1H and ^{13}C NMR data, Tables 3 and 4; HRESIMS *m/z* 285.1691 $[M + H]^+$ (calcd for $C_{15}H_{25}O_5$ (+1) 285.1697); 307.1512 $[M + Na]^+$ (calcd for $C_{15}H_{24}O_5Na$ (+1) 307.1516); 267.1583 $(M + H)^+[-H_2O]$ (calcd for $C_{15}H_{23}O_4$ (+1) 267.1591).

Biological Assays. *Cell Culture.* Tetracycline (Tet)-inducible HEK293-TREx cells stably transfected with HA-tagged human TRPM7 wild type and TRPM2 wild type were cultured in DMEM medium (Sigma) containing 10% fetal bovine serum (FBS) (Corning), blasticidin (5 μg/mL) (Gibco), and zeocin (0.4 mg/mL) (Gibco). Overexpression was induced by adding 1 μg/mL tetracycline (Gibco) to the culture medium. Patch-clamp current measurements of TRPM7 were performed 18−22 h post-tetracycline induction. For TRPM2, patch-clamp was performed 4−6 h after tetracycline induction. Cells were maintained at 37 °C under 95% air and 5% CO_2 conditions.

Electrophysiology. For the whole-cell patch-clamp technique assessing overexpressed TRPM7 and TRPM2, the extracellular solution contained (in mM) 140 NaCl, 2.8 KCl, 2 $MgCl_2$, 1 $CaCl_2$, 10 HEPES-NaOH, and 10 glucose (pH 7.2, 300 mOsm). Intracellular pipet-filling solutions for TRPM7 contained (in mM) 120 K-glutamate, 8 NaCl, 1.5 Mg-ATP, 1.5 $MgCl_2$ (300 μM free Mg^{2+}), 10 BAPTA (1,2-bis(*o*-aminophenoxy)ethane-*N*,*N*,*N*′,*N*′-tetraacetic acid), and 10 HEPES-KOH (pH 7.2, 300 mOsm). For TRPM2, intracellular solution contained (in mM) 120 K-glutamate, 8 NaCl, 1 $MgCl_2$, 0.1 ADPR (adenosine diphosphate ribose), and 10 HEPES-KOH (pH 7.2, 300mOsm). Free intracellular Mg^{2+} concentration was calculated with WebMaxC Standard.

Patch-clamp experiments were performed in the whole-cell configuration. TRPM7 and TRPM2 currents were elicited by a ramp protocol from −100 mV to +100 mV from a holding potential of 0 mV over 50 ms and acquired at 0.5 kHz. Inward current amplitudes over the course of the experiment were extracted at −80 mV, outward currents at +80 mV, and plotted versus time. Data were normalized to cell capacitance measured immediately after whole-cell break-in as pA/pF. Capacitance was measured using the automated capacitance cancellation function of the EPC-9 (HEKA). All values are given as mean ± standard error of the mean. Patch pipets (Sutter Instrument) were pulled and polished and had a tip resistance of 2−3 MΩ with the solutions used.

Computational Methods. For NMR prediction, the computational work was guided by *Nature Protocols*[37] with updated Python scripts.[38] Conformers within 5 kcal/mol of the lowest energy conformer were searched using the Monte Carlo multiple minimum (MCMM) method[39] and the OPLS-2005 force field[40] in MacroModel[41] (Schrodinger Inc.). Each conformer within 5 kcal/mol of the lowest energy conformer was optimized in Gaussian 09[42] at the M06-2X[43] /6-311+G(d,p) level with a polarizable continuum model (PCM)[44] for MeOH or $CHCl_3$, and the geometries of all conformers with similar energies were checked for redundancy after removal of any conformer with an imaginary frequency. NMR shielding tensors of all unique conformers within the energy window were computed using the gauge-independent atomic orbital (GIAO)[45] method at the B3LYP[46] /6-311+G(2d,p)[47,48] level with PCM, and ^1H and ^{13}C chemical shifts were obtained after applying appropriate scaling factors (^1H: intercept = 31.9477, slope = −1.0767; ^{13}C: intercept = 181.2412, slope = −1.0522). Statistical comparisons of the computed shifts with the experimental data were carried out using either the spreadsheet for DP4+ analysis[23] with both scaled and unscaled values or the applet for CP3 analysis.[49]

For ECD prediction, the previous applies, but time-dependent density functional theory (TDDFT)[20,21] was conducted at the BHandHLYP[50] /def2-TZVPP level for compounds **1**−**4**, but for **5**−**7** conformers were optimized at the CAM-B3LYP[51] /6-31+G(d,p)[48,52−54] level and TDDFT calculations were conducted at the CAM-B3LYP[51]/def2-TZVPP level to calculate the electronic excitation energies and rotational strengths with PCM in MeOH. These methods have been proven to be able to generate accurate ECD predictions for similar molecules.[55] Boltzmann-weighted ECD spectra, where conformers with >1.5% contribution were checked for redundancy, were calculated using SpecDis[22] for comparison by similarity factor with the experimentally determined data recorded in MeOH.

■ ASSOCIATED CONTENT

Supporting Information

The Supporting Information is available free of charge at https://pubs.acs.org/doi/10.1021/acs.jnatprod.1c01014.

Copies of the ^1H, ^{13}C, and 2D NMR spectroscopic data, along with IR, UV, ECD, and UV for purity for all new compounds; for computation regarding compounds **1** and **3**−**7**, Boltzmann distribution, XYZ coordinates and images of conformers accompanied by the conformational analysis; bioassay data for TRPM ion channels (PDF)

NMR fid files (ZIP)

■ AUTHOR INFORMATION

Corresponding Author

Philip G. Williams − *Department of Chemistry, University of Hawai'i at Manoa, Honolulu, Hawaii 96822, United States;* orcid.org/0000-0001-8987-0683; Phone: 808 956 5720; Email: philipwi@hawaii.edu; Fax: 808 956 5908

Authors

Timothy J. O'Donnell − *Department of Chemistry, University of Hawai'i at Manoa, Honolulu, Hawaii 96822, United States*

Yuheng Luo − *Department of Chemistry, University of Hawai'i at Manoa, Honolulu, Hawaii 96822, United States;* orcid.org/0000-0002-3124-1179

Wesley Y. Yoshida − *Department of Chemistry, University of Hawai'i at Manoa, Honolulu, Hawaii 96822, United States*

Sayuri Suzuki − *Center for Biomedical Research, The Queen's Medical Center, Honolulu, Hawaii 96813, United States*

Rui Sun − *Department of Chemistry, University of Hawai'i at Manoa, Honolulu, Hawaii 96822, United States;* orcid.org/0000-0003-0638-1353

Complete contact information is available at: https://pubs.acs.org/10.1021/acs.jnatprod.1c01014

Notes

The authors declare no competing financial interest.

■ ACKNOWLEDGMENTS

This work was supported by NIH grant 5R01AG039468 to P.W. Funds for the upgrades of the NMR instrumentation were provided by the CRIF program of the National Science Foundation (CH E9974921), the Elsa Pardee Foundation, and the University of Hawaii at Manoa. The purchase of the Agilent TOF LC-MS was funded by grant W911NF-04-1-0344 from the Department of Defense, and the purchase of the Agilent QTOF LC-MS was funded by MRI grant 1532310 from the National Science Foundation. The computation was carried out at the information technology service (ITS) from the University of Hawai'i, Manoa.

■ REFERENCES

(1) Demay, J.; Bernard, C.; Reinhardt, A.; Marie, B. *Mar. Drugs* **2019**, *17* (6), 320.
(2) Gerwick, W. H.; Tan, L. T.; Sitachitta, N. *Alkaloids Chem. Biol.* **2001**, *57*, 75−184.
(3) Engene, N.; Gunasekera, S. P.; Gerwick, W. H.; Paul, V. J. *Appl. Environ. Microbiol.* **2013**, *79* (6), 1882−1888.
(4) Penner, R.; Fleig, A. *Handb. Exp. Pharmacol.* **2007**, *179* (179), 313−328.
(5) Hughes, R.-A.; Miller, E. S.; Zhang, Y.; Zhang, R.; Lindsey, J. S.; Williams, P. G. Genome Sequence and Composition of a Tolyporphin-Producing Cyanobacterium-Microbial Community. *Appl. Environ. Microbiol.* **2017**, *83*, DOI: 10.1128/AEM.01068-17
(6) Anderson, R. C.; Gunn, D. M.; Murray-Rust, J.; Murray-Rust, P.; Roberts, J. S. *J. Chem. Soc., Chem. Commun.* **1977**, 27−28.
(7) Malmberg, A. G. *Phytochem.* **1982**, *21* (7), 1818−1819.
(8) Spreitzer, H.; Piringer, I.; Holzer, W.; Widhalm, M. *Helv. Chim. Acta* **1998**, *81* (12), 2292−2299.
(9) Engstrom, K. *Phytochem.* **1998**, *47*, 985−990.
(10) Kuroyanagi, M.; Arakawa, T.; Mikami, Y.; Yoshida, K.; Kawahar, N.; Hayashi, T.; Ishimaru, H. *J. Nat. Prod.* **1998**, *61* (12), 1516−1519.
(11) Ueda, J. Y.; Imamura, L.; Tezuka, Y.; Tran, Q. L.; Tsuda, M.; Kadota, S. *Bioorg. Med. Chem.* **2006**, *14* (10), 3571−3574.
(12) Kawauchi, M.; Arima, T.; Shirota, O.; Sekita, S.; Nakane, T.; Takase, Y.; Kuroyanagi, M. *Chem. Pharm. Bull. (Tokyo).* **2010**, *58* (7), 934−938.
(13) Kamauchi, H.; Kinoshita, K.; Takatori, K.; Sugita, T.; Takahashi, K.; Koyama, K. *Tetrahedron* **2015**, *71* (13), 1909−1914.
(14) Zhang, L.; Li, G.-S.; Yao, F.; Yue, X.-D.; Dai, S.-J. *Phytochem. Lett.* **2015**, *11*, 173−176.
(15) Jakupovic, J.; Lehmann, L.; Bohlmann, F.; King, R. M.; Robinson, H. *Phytochem.* **1988**, *27* (12), 3831−3839.
(16) Engstrom, K. *Phytochem.* **1998**, *49* (6), 1585−1587.
(17) Yuan, P.; Guo, F.; Zheng, K.; Chen, K.; Jia, Q.; Li, Y. *Nat. Prod. Res.* **2016**, *30* (15), 1682−1689.
(18) Gawroński, J. K. *Tetrahedron* **1982**, *38* (1), 3−26.
(19) Kirk, D. N. *Tetrahedron* **1986**, *42* (3), 777−818.
(20) Runge, E.; Gross, E. K. U. *Phys. Rev. Lett.* **1984**, *52* (12), 997−1000.
(21) Gross, E. K. U.; Dobson, J. F.; Petersilka, M. *Top. Curr. Chem.* **1996**, *181*, 81−159.
(22) Bruhn, T.; Schaumlöffel, A.; Hemberger, Y. *SpecDis version 1.63*; University of Wuerzburg: Germany, 2015.
(23) Grimblat, N.; Zanardi, M. M.; Sarotti, A. M. *J. Org. Chem.* **2015**, *80* (24), 12526−12534.
(24) Williamson, K. L.; Howell, T.; Spencer, T. A. *J. Am. Chem. Soc.* **1966**, *88* (2), 325−334.
(25) About 21% of the conformers with > 1% abundance had these protons only 2.28 Å apart, which presumably accounts for the stronger than expected NOE.
(26) Afiyatullov, S. S.; Leshchenko, E. V.; Sobolevskaya, M. P.; Antonov, A. S.; Denisenko, V. A.; Popov, R. S.; Khudyakova, Y. V.; Kirichuk, N. N.; Kuz'mich, A. S.; Pislyagin, E. A.; Kim, N. Y.; Berdyshev, D. V. *Chem. Nat. Compd.* **2017**, *53* (2), 290−294.
(27) de Pascual-T, J.; Bellido, I. S.; González, M. S. *Tetrahedron* **1980**, *36* (3), 371−376.
(28) Hikino, H.; Aota, K.; Kuwano, D.; Takemoto, T. *Tetrahedron* **1971**, *27* (19), 4831−4836.
(29) Hikino, H.; Aota, K.; Kuwano, D.; Takemoto, T. *Tetrahedron Lett.* **1969**, *10* (32), 2741−2742.
(30) Babidge, P. J.; Massy-Westropp, R. A. *Aust. J. Chem.* **1984**, *37* (3), 629−633.
(31) Bagchi, A.; Oshima, Y.; Hikino, H. *Planta Med.* **1991**, *57*, 282−283.
(32) Fujioka, T.; Yamamoto, M.; Kashiwada, Y.; Fujii, H.; Mihashi, K.; Ikeshiro, Y.; Chen, I.-S.; Lee, K.-H. *Bioorg. Med. Chem. Lett.* **1998**, *8* (24), 3479−3482.
(33) Ding, L.; Maier, A.; Fiebig, H. H.; Lin, W. H.; Peschel, G.; Hertweck, C. *J. Nat. Prod.* **2012**, *75* (12), 2223−2227.
(34) Gu, J.; Qian, S. Y.; Zhao, Y. L.; Cheng, G. G.; Hu, D. B.; Zhang, B. H.; Li, Y.; Liu, Y. P.; Luo, X. D. *Tetrahedron* **2014**, *70* (6), 1375−1382.
(35) Afiyatullov, S. S.; Leshchenko, E. V.; Sobolevskaya, M. P.; Denisenko, V. A.; Kirichuk, N. N.; Khudyakova, Y. V.; Hoai, T. P. T.; Dmitrenok, P. S.; Menchinskaya, E. S.; Pislyagin, E. A.; Berdyshev, D. V. *Phytochem. Lett.* **2015**, *14*, 209−214.
(36) Burnett, R. D.; Kirk, D. N. *J. Chem. Soc., Perkin Trans. 1* **1981**, 1460−1468.
(37) Willoughby, P. H.; Jansma, M. J.; Hoye, T. R. *Nat. Protoc.* **2014**, *9* (3), 643−660.
(38) Bhandari Neupane, J.; Neupane, R. P.; Luo, Y.; Yoshida, W. Y.; Sun, R.; Williams, P. G. *Org. Lett.* **2019**, *21* (20), 8449−8453.
(39) Li, Z.; Scheraga, H. A. *Proc. Natl. Acad. Sci. U. S. A.* **1987**, *84* (19), 6611−6615.
(40) Kaminski, G. A.; Friesner, R. A.; Tirado-Rives, J.; Jorgensen, W. L. *J. Phys. Chem. B* **2001**, *105* (28), 6474−6487.
(41) *MacroModel, S.*; MacroModel LLC: New York, NY, 2019.
(42) Frisch, M. J.; Trucks, G. W.; Schlegel, H. B.; Scuseria, G. E.; Robb, M. A.; Cheeseman, J. R.; Scalmani, G.; Barone, V.; Mennucci, B.; Petersson, G. A.; Nakatsuji, H.; Caricato, M.; Li, X.; Hratchian, H. P.; Izmaylov, A. F.; Bloino, J.; Zheng, G.; Sonnenberg, J. L.; Hada, M.; Ehara, M.; Toyota, K.; Fukuda, R.; Hasegawa, J.; Ishida, M.; Nakajima, T.; Honda, Y.; Kitao, O.; Nakai, H.; Vreven, T.; Montgomery, J. A.; Peralta, J. E.; Ogliaro, F.; Bearpark, M.; Heyd, J. J.; Brothers, E.; Kudin, K. N.; Staroverov, V. N.; Kobayashi, R.; Normand, J.; Raghavachari, K.; Rendell, A.; Burant, J. C.; Iyengar, S. S.; Tomasi, J.; Cossi, M.; Rega, N.; Millam, J. M.; Klene, M.; Knox, J. E.; Cross, J. B.; Bakken, V.; Adamo, C.; Jaramillo, J.; Gomperts, R.; Stratmann, R. E.; Yazyev, O.; Austin, A. J.; Cammi, R.; Pomelli, C.; Ochterski, J. W.; Martin, R. L.; Morokuma, K.; Zakrzewski, V. G.; Voth, G. A.; Salvador, P.; Dannenberg, J. J.; Dapprich, S.; Daniels, A. D.; Farkas; Foresman, J. B.; Ortiz, J. V.; Cioslowski, J.; Fox, D. J. *Gaussian 09*, Revision B.01; Gaussian Inc.: Wallingford, CT, 2009.
(43) Zhao, Y.; Truhlar, D. G. *Theor. Chem. Acc.* **2008**, *120* (1), 215−241.
(44) Tomasi, J.; Mennucci, B.; Cammi, R. *Chem. Rev.* **2005**, *105* (8), 2999−3094.
(45) Cramer, C. J. *Essentials of Computational Chemistry: Theories and Models*, 2nd ed.; John Wiley & Sons: Chichester, England, 2004; p 614.
(46) Becke, A. D. *Phys. Rev. A* **1988**, *38* (6), 3098−3100.

(47) Krishnan, R.; Binkley, J. S.; Seeger, R.; Pople, J. A. *J. Chem. Phys.* **1980**, *72* (1), 650−654.
(48) Clark, T.; Chandrasekhar, J.; Spitznagel, G. W.; Schleyer, P. V. R. *J. Comput. Chem.* **1983**, *4* (3), 294−301.
(49) Smith, S. G.; Goodman, J. M. *J. Org. Chem.* **2009**, *74* (12), 4597−4607.
(50) Becke, A. D. *J. Chem. Phys.* **1993**, *98* (2), 1372−1377.
(51) Yanai, T.; Tew, D. P.; Handy, N. C. *Chem. Phys. Lett.* **2004**, *393* (1), 51−57.
(52) Ditchfield, R.; Hehre, W. J.; Pople, J. A. *J. Chem. Phys.* **1971**, *54* (2), 724−728.
(53) Hehre, W. J.; Ditchfield, R.; Pople, J. A. *J. Chem. Phys.* **1972**, *56* (5), 2257−2261.
(54) Hariharan, P. C.; Pople, J. A. *Theor. Chim. Acta* **1973**, *28* (3), 213−222.
(55) Weigend, F.; Ahlrichs, R. *Phys. Chem. Chem. Phys.* **2005**, *7* (18), 3297−3305.

https://doi.org/10.1021/acs.jnatprod.1c01014
J. Nat. Prod. 2022, 85, 415−425